Computers and Mathematics with Applications 75 (2018) 1912–1928

Contents lists available at ScienceDirect

Computers and Mathematics with Applications

journal homepage: www.elsevier.com/locate/camwa

Convergence analysis and numerical implementation of a second order numerical scheme for the three-dimensional phase field crystal equation

Lixiu Dong [a], Wenqiang Feng [b,*], Cheng Wang [c], Steven M. Wise [b], Zhengru Zhang [a]

[a] School of Mathematical Sciences, Beijing Normal University, Beijing 100875, PR China
[b] Department of Mathematics, The University of Tennessee, Knoxville, TN 37996, United States
[c] Department of Mathematics, The University of Massachusetts, North Dartmouth, MA 02747, United States

ARTICLE INFO

Article history:
Available online 10 August 2017

Keywords:
Three-dimensional phase field crystal
Finite difference
Energy stability
Second order numerical scheme
Convergence analysis
Nonlinear multigrid solver

ABSTRACT

In this paper we analyze and implement a second-order-in-time numerical scheme for the three-dimensional phase field crystal (PFC) equation. The numerical scheme was proposed in Hu et al. (2009), with the unique solvability and unconditional energy stability established. However, its convergence analysis remains open. We present a detailed convergence analysis in this article, in which the maximum norm estimate of the numerical solution over grid points plays an essential role. Moreover, we outline the detailed multigrid method to solve the highly nonlinear numerical scheme over a cubic domain, and various three-dimensional numerical results are presented, including the numerical convergence test, complexity test of the multigrid solver and the polycrystal growth simulation.

1. Introduction

Defects, such as vacancies, grain boundaries, and dislocations, are observed in crystalline materials, and a precise and accurate understanding of their formation and evolution is of great interest. The phase field crystal (PFC) model was proposed in [1] as a new approach to simulate crystal dynamics at the atomic scale in space but on diffusive scales in time. This model naturally incorporates elastic and plastic deformations, multiple crystal orientations and defects and has already been used to simulate a wide variety of microstructures, such as epitaxial thin film growth [2], grain growth [3], eutectic solidification [4], and dislocation formation and motion [3,5]. The idea is that the phase variable describes a coarse-grained temporal average of the number density of atoms, and the approach can be related to dynamic density functional theory [6,7]. The method represents a significant advantage over other atomistic methods, such as molecular dynamics methods where the time steps are constrained by atomic-vibration time scales. More detailed descriptions are available in [3,8,9], and the related works for the amplitude expansion approach could be found in [8,10].

Consider the dimensionless energy of the form [1,2,11]:

$$E(\phi) = \int_{\Omega} \left[\frac{1}{4}\phi^4 + \frac{1-\varepsilon}{2}\phi^2 - |\nabla\phi|^2 + \frac{1}{2}(\Delta\phi)^2 \right] d\mathbf{x}, \tag{1.1}$$

* Corresponding author.
E-mail addresses: 201421130036@mail.bnu.edu.cn (L. Dong), wfeng1@utk.edu (W. Feng), cwang1@umassd.edu (C. Wang), swise@math.utk.edu (S.M. Wise), zrzhang@bnu.edu.cn (Z. Zhang).

http://dx.doi.org/10.1016/j.camwa.2017.07.012
0898-1221/

where $\Omega = (0, L_x) \times (0, L_y) \times (0, L_z) \subset \mathbb{R}^3$, $\phi : \Omega \to \mathbb{R}$ is the atom density field, and $\varepsilon > 0$ is a constant. We assume that ϕ is periodic on Ω. The PFC equation [1,2] is given by the H^{-1} gradient flow associated with the energy (1.1):

$$\begin{aligned} &\phi_t = \nabla \cdot (M(\phi)\nabla\mu), \quad \text{in } \Omega_T = \Omega \times (0, T), \\ &\mu = \delta_\phi E = \phi^3 + (1-\varepsilon)\phi + 2\Delta\phi + \Delta^2\phi, \quad \text{in } \Omega_T, \\ &\phi(x, y, z, 0) = \phi_0(x, y, z), \quad \text{in } \Omega. \end{aligned} \tag{1.2}$$

in which $M(\phi) > 0$ is a mobility and μ is the chemical potential. Periodic boundary conditions are imposed for $\Delta\phi$ and μ.

The PFC equation is a high-order (sixth-order) nonlinear partial differential equation. Regarding the PDE analysis, existence and uniqueness of a global-in-time strong solution and smooth solution for the modified phase field crystal (MPFC) equation – which generalizes the PFC equations and includes a second order temporal derivative $\beta\phi_{tt}$ – has been established in a recent work [12]. In more detail, it was proved that, for any H^m ($m \geq 3$) initial data (for the phase variable ϕ), there is an H^m estimate for the solution at any time $T > 0$, so that a global-in-time strong solution and smooth solution is available, dependent on the regularity of the initial data. Such an analysis could be easily extended to the case with $\beta = 0$, corresponding to the parabolic PFC equation. Therefore, one could always assume the existence and uniqueness of the solution for the PFC equation (1.2), if the initial data has a regularity of at least H^3.

There have been some related works to develop numerical schemes for the PFC equation. Cheng and Warren [13] introduced a linearized spectral scheme, similar to one for the Cahn–Hilliard equation analyzed in [14]. This scheme is not expected to be provably unconditionally energy stable. The finite element PFC method of Backofen et al. [6] employs what is essentially a standard backward Euler scheme, but where the nonlinear term ϕ^3 in the chemical potential is linearized via $(\phi^{k+1})^3 \approx 3(\phi^k)^2\phi^{k+1} - 2(\phi^k)^3$. Both energy stability and solvability are issues for this scheme, because the term $2\Delta\phi$ is implicit in the chemical potential. Tegze et al. [15] developed a semi-implicit spectral scheme for the binary PFC equations that is not expected to unconditionally stable. Also see other related numerical works [16–19] in recent years.

The energy stability of a numerical scheme has always been a very important issue, since it plays an essential role in the accuracy of long time numerical simulation. The standard convex splitting scheme, originated from Eyre's work [20], has been a well-known approach to achieve numerical energy stability. In this framework, the convex part of the chemical potential is treated implicitly, while the concave part is updated explicitly. A careful analysis leads to the unique solvability and unconditional energy stability of the numerical scheme, unconditionally with respect to the time and space step sizes. Such an idea has been applied to a wide class of gradient flows in recent years, and both first and second order accurate in time algorithms have been developed. See the related works for the PFC equation and the modified PFC (MPFC) equation [12,21–27].

On the other hand, a well-known drawback of the first order convex splitting approach is that an extra dissipation has been added to ensure unconditional stability; in turn, the first order numerical approach introduces a significant amount of numerical error [28]. For this reason, second-order energy stable methods have been highly desirable.

There have been other related works of "energy stable" schemes for the certain gradient flows in recent years. For example, an alternate variable is used in [29], denoted as a second order approximation to $v = \phi^2 - 1$ in the Cahn–Hilliard model. A linearized, second order accurate scheme is derived as the outcome of this idea, and the stability is established for a modified energy. A similar idea has been applied to the PFC model in a more recent article [30]. However, such an energy stability is applied to a pair of numerical variables (ϕ, v), and an H^2 stability for the original physical variable ϕ has not been justified. As a result, the convergence analysis is not available for this numerical approach. Similar methodology has been reported in the invariant energy quadratization (IEQ) approach [31–33], etc.

In comparison, a second order numerical scheme was proposed and studied for the PFC equation in [21]. By a careful choice of the second order temporal approximations to each term in the chemical potential, the unique solvability and unconditional energy were justified at a theoretical level, with the centered difference discretization taken in space. In particular, this energy stability is derived with respect to the original energy functional, combined with an auxiliary, non-negative correction term, so that a uniform in time H^2 bound is available for the numerical solution. Meanwhile, a detailed convergence analysis has not been theoretically reported for the proposed second order scheme, although the full convergence order was extensively demonstrated in the numerical experiments. The key difficulty in the convergence analysis is associated with the maximum norm bound estimate for the numerical solution, and such a bound plays an essential role in the theoretical convergence derivation. In more details, the unconditional energy stability indicates a uniform in time H^2 bound of the numerical solution at a discrete level. Although the Sobolev embedding from H^2 to L^∞ is straightforward in three-dimensional space, a direct estimate for the corresponding grid function is not directly available. In two-dimensional space, such a discrete Sobolev embedding has been proved in the earlier works [21,27], using complicated calculations of the difference operators. However, as stated in Remark 12 of [21], *"the proof presented in* [27] *does not automatically extend to three dimensions. This is because a discrete Sobolev inequality is used to translate energy stability into point-wise stability, and the inequality fails in three dimensions. We are currently studying the three dimensional case in further detail".*

In this paper, we provide a detailed convergence analysis for the fully discrete scheme formulated in [21], which is shown to be second order accurate in both time and space. In particular, the maximum norm estimate of the three-dimensional numerical solution is accomplished via a discrete Fourier transformation over a uniform numerical grid, so that the discrete Parseval equality is valid. And also, the equivalence between the discrete and continuous H^2 norms for the numerical grid function and its continuous version, respectively, can be established. In turn, the discrete Sobolev inequality is obtained from its continuous version. Such an ℓ^∞ bound of the discrete numerical solution is crucial, so that the convergence analysis

could go through for the scheme. Moreover, the Crank–Nicolson approximation to the surface diffusion term poses another challenge in the convergence proof, since the diffusion coefficients at time steps t^{k+1} and t^k are equally distributed, in comparison with an alternate second order approximation reported in a few recent works [34,35], in which the diffusion coefficients are distributed at time steps t^{k+1} and t^{k-1}, respectively. To overcome this difficulty, we have to perform an error analysis at time instant $t^{k+1/2}$, in combination with a subtle estimate for the numerical error in the concave diffusion term.

In addition, we also present various numerical simulation results of three-dimensional PFC model in this article. It is noted that most numerical results for the PFC equation reported in the existing literature are two-dimensional, or over a two-dimensional surface; see [13,21,22,36–38], etc. For a gradient flow in which the nonlinear terms take a form of ϕ^3 pattern, great efficiency and accuracy of the nonlinear multi-grid solver have been extensively demonstrated in the numerical experiments; see the related works [21,22,35,39–42]. We apply the nonlinear multi-grid algorithm to implement the three-dimensional numerical scheme; its great numerical efficiency enables us to compute the three-dimensional model using local servers. Both the numerical accuracy check and the detailed numerical simulation results of three-dimensional polycrystal growth are reported.

The rest of paper is organized as follows. In Section 2, we introduce the finite difference spatial discretization in three-dimensional space, and review a few preliminary estimates. In Section 3 we review the second order numerical scheme proposed in [21], and state the main theoretical results. The detailed convergence proof is given in Section 4. Furthermore, the details of the three-dimensional multi-grid solver is outlined in Section 5. Subsequently, the numerical results are presented in Section 6. Finally, some concluding remarks are made in Section 7.

2. Finite difference discretization and a few preliminary estimates

For simplicity of presentation, we denote $(\cdot,\cdot)$ as the standard L^2 inner product, and $\|\cdot\|$ as the standard L^2 norm, and $\|\cdot\|_{H^m}$ as the standard H^m norm. We use the notation and results for some discrete functions and operators from [27,35,42]. Let $\Omega = (0, L_x) \times (0, L_y) \times (0, L_z)$, where for simplicity, we assume $L_x = L_y = L_z =: L > 0$. It is also assumed that $h_x = h_y = h_y = h$ and we denote $L = m \cdot h$, where m is a positive integer. The parameter $h = \frac{L}{m}$ is called the mesh or grid spacing. We define the following two uniform, infinite grids with grid spacing $h > 0$:

$$E := \left\{ \xi_{i+\frac{1}{2}} | i \in \mathbb{Z} \right\}, \qquad C := \{ \xi_i | i \in \mathbb{Z} \},$$

where $\xi_i = \xi(i) := (i - \frac{1}{2}) \cdot h$. Consider the following 3D discrete periodic function spaces:

$$\mathcal{C}_{\text{per}} := \left\{ \nu : C \times C \times C \to \mathbb{R} \,\middle|\, \nu_{i,j,k} = \nu_{i+\alpha m, j+\beta m, k+\gamma m},\ \forall\, i,j,k,\alpha,\beta,\gamma \in \mathbb{Z} \right\},$$

$$\mathcal{E}^{\text{x}}_{\text{per}} := \left\{ \nu : E \times C \times C \to \mathbb{R} \,\middle|\, \nu_{i+\frac{1}{2},j,k} = \nu_{i+\frac{1}{2}+\alpha m, j+\beta m, k+\gamma m},\ \forall\, i,j,k,\alpha,\beta,\gamma \in \mathbb{Z} \right\}.$$

The spaces $\mathcal{E}^{\text{y}}_{\text{per}}$ and $\mathcal{E}^{z}_{\text{per}}$ are analogously defined. The functions of $\mathcal{C}_{\text{per}}$ are called *cell centered functions*. The functions of $\mathcal{E}^{\text{x}}_{\text{per}}$, $\mathcal{E}^{\text{y}}_{\text{per}}$, and $\mathcal{E}^{z}_{\text{per}}$, are called *east–west face-centered functions*, *north–south face-centered functions*, and *up-down face-centered functions*, respectively. We also define the mean zero space

$$\mathcal{C}_{\text{per}} := \left\{ \nu \in \mathcal{C}_{\text{per}} \,\middle|\, \overline{\nu} := \frac{h^3}{|\Omega|} \sum_{i,j,k=1}^{m} \nu_{i,j,k} = 0 \right\}.$$

We now introduce the important difference and average operators on the spaces:

$$A_x \nu_{i+\frac{1}{2},j,k} := \frac{1}{2}\left(\nu_{i+1,j,k} + \nu_{i,j,k}\right), \qquad D_x \nu_{i+\frac{1}{2},j,k} := \frac{1}{h}\left(\nu_{i+1,j,k} - \nu_{i,j,k}\right),$$

$$A_y \nu_{i,j+\frac{1}{2},k} := \frac{1}{2}\left(\nu_{i,j+1,k} + \nu_{i,j,k}\right), \qquad D_y \nu_{i,j+\frac{1}{2},k} := \frac{1}{h}\left(\nu_{i,j+1,k} - \nu_{i,j,k}\right),$$

$$A_z \nu_{i,j,k+\frac{1}{2}} := \frac{1}{2}\left(\nu_{i,j,k+1} + \nu_{i,j,k}\right), \qquad D_z \nu_{i,j,k+\frac{1}{2}} := \frac{1}{h}\left(\nu_{i,j,k+1} - \nu_{i,j,k}\right),$$

with $A_x,\ D_x : \mathcal{C}_{\text{per}} \to \mathcal{E}^{\text{x}}_{\text{per}}, A_y,\ D_y : \mathcal{C}_{\text{per}} \to \mathcal{E}^{\text{y}}_{\text{per}}, A_z,\ D_z : \mathcal{C}_{\text{per}} \to \mathcal{E}^{z}_{\text{per}}$. Likewise,

$$a_x \nu_{i,j,k} := \frac{1}{2}\left(\nu_{i+\frac{1}{2},j,k} + \nu_{i-\frac{1}{2},j,k}\right), \qquad d_x \nu_{i,j,k} := \frac{1}{h}\left(\nu_{i+\frac{1}{2},j,k} - \nu_{i-\frac{1}{2},j,k}\right),$$

$$a_y \nu_{i,j,k} := \frac{1}{2}\left(\nu_{i,j+\frac{1}{2},k} + \nu_{i,j-\frac{1}{2},k}\right), \qquad d_y \nu_{i,j,k} := \frac{1}{h}\left(\nu_{i,j+\frac{1}{2},k} - \nu_{i,j-\frac{1}{2},k}\right),$$

$$a_z \nu_{i,j,k} := \frac{1}{2}\left(\nu_{i,j,k+\frac{1}{2}} + \nu_{i,j,k-\frac{1}{2}}\right), \qquad d_z \nu_{i,j,k} := \frac{1}{h}\left(\nu_{i,j,k+\frac{1}{2}} - \nu_{i,j,k-\frac{1}{2}}\right),$$

with $a_x,\ d_x : \mathcal{E}^{\mathrm{x}}_{\mathrm{per}} \to \mathcal{C}_{\mathrm{per}}$, $a_y,\ d_y : \mathcal{E}^{\mathrm{y}}_{\mathrm{per}} \to \mathcal{C}_{\mathrm{per}}$, and $a_z,\ d_z : \mathcal{E}^{z}_{\mathrm{per}} \to \mathcal{C}_{\mathrm{per}}$. The standard 3D discrete Laplacian, $\Delta_h : \mathcal{C}_{\mathrm{per}} \to \mathcal{C}_{\mathrm{per}}$, is given by

$$\begin{aligned}\Delta_h v_{i,j,k} &:= d_x(D_x v)_{i,j,k} + d_y(D_y v)_{i,j,k} + d_z(D_z v)_{i,j,k}\\ &= \frac{1}{h^2}\left(v_{i+1,j,k} + v_{i-1,j,k} + v_{i,j+1,k} + v_{i,j-1,k} + v_{i,j,k+1} + v_{i,j,k-1} - 6v_{i,j,k}\right).\end{aligned}$$

Now we are ready to define the following grid inner products:

$$\begin{aligned}&(v,\xi)_2 := h^3 \sum_{i,j,k=1}^{m} v_{i,j,k}\xi_{i,j,k}, \quad v,\ \xi \in \mathcal{C}_{\mathrm{per}},\ [v,\xi]_{\mathrm{x}} := (a_x(v\xi),1)_2, \quad v,\ \xi \in \mathcal{E}^{\mathrm{x}}_{\mathrm{per}},\\ &[v,\xi]_{\mathrm{y}} := \left(a_y(v\xi),1\right)_2, \quad v,\ \xi \in \mathcal{E}^{\mathrm{y}}_{\mathrm{per}}, \qquad [v,\xi]_{z} := (a_z(v\xi),1)_2, \quad v,\ \xi \in \mathcal{E}^{z}_{\mathrm{per}}.\end{aligned}$$

We now define the following norms for cell-centered functions. If $v \in \mathcal{C}_{\mathrm{per}}$, then $\|v\|_2^2 := (v,v)_2$; $\|v\|_p^p := \left(|v|^p,1\right)_2$ $(1 \le p < \infty)$, and $\|v\|_\infty := \max_{1\le i,j,k\le m}\left|v_{i,j,k}\right|$. Similarly, we define the gradient norms: for $v \in \mathcal{C}_{\mathrm{per}}$,

$$\|\nabla_h v\|_2^2 := [D_x v, D_x v]_{\mathrm{x}} + \left[D_y v, D_y v\right]_{\mathrm{y}} + [D_z v, D_z v]_{z}.$$

Consequently,

$$\|v\|_{2,2}^2 := \|v\|_2^2 + \|\nabla_h v\|_2^2 + \|\Delta_h v\|_2^2.$$

In addition, the discrete energy $F_h(\phi) : \mathcal{C}_{\mathrm{per}} \to \mathbb{R}$ is defined as

$$F_h(\phi) = \frac{1}{4}\|\phi\|_4^4 + \frac{1-\varepsilon}{2}\|\phi\|_2^2 - \|\nabla_h\phi\|_2^2 + \frac{1}{2}\|\Delta_h\phi\|_2^2. \tag{2.1}$$

The following preliminary estimates are cited from earlier works. For more details we refer the reader to [21,27].

Lemma 2.1. *For any $f, g \in \mathcal{C}_{\mathrm{per}}$, the following summation by parts formulas are valid:*

$$(f, \Delta_h g) = -(\nabla_h f, \nabla_h g), \qquad (f, \Delta_h^2 g) = (\Delta_h f, \Delta_h g), \qquad (f, \Delta_h^3 g) = -(\nabla_h \Delta_h f, \nabla_h \Delta_h g). \tag{2.2}$$

Lemma 2.2. *Suppose $\phi \in \mathcal{C}_{\mathrm{per}}$. Then*

$$\|\Delta_h\phi\|_2^2 \le \frac{1}{3\alpha^2}\|\phi\|_2^2 + \frac{2\alpha}{3}\|\nabla_h(\Delta_h\phi)\|_2^2, \tag{2.3}$$

is valid for arbitrary $\alpha > 0$.

Lemma 2.3. *For $\phi \in \mathcal{C}_{\mathrm{per}}$, we have the estimate*

$$F_h(\phi) \ge C\|\phi\|_{2,2}^2 - \frac{L^3}{4}, \tag{2.4}$$

with C only dependent on Ω, and $F_h(\phi)$ given by (2.1).

3. The fully discrete second order numerical scheme and the main results

Let $N_t \in \mathbb{Z}^+$, and set $\tau := T/N_t$, where T is the final time. For our present and future use, we define the canonical grid projection operator $\mathsf{P}_h : C^0_{\mathrm{per}}(\Omega) \to \mathcal{C}_{\mathrm{per}}$ via $[\mathsf{P}_h v]_{i,j,k} = v(\xi_i,\xi_j,\xi_k)$. Set $v_{h,s} := \mathsf{P}_h u(\cdot, s)$. Then $F_h(v_{h,s}) + \frac{1}{2}\|\nabla_h(v_{h,s} - v_{h,0})\|_2^2 \to E(u(\cdot,0))$ as $h \to 0$ and $s \to 0$ for sufficiently regular v. We denote ϕ_e as the exact (periodic) solution to the PFC equation (1.2) and take $\Phi^\ell := \mathsf{P}_h\phi_e(\cdot, t_\ell)$.

Our second order numerical scheme in [21] can be formulated as follows: for $1 \le \kappa \le N_t - 1$, given $\phi^\kappa, \phi^{\kappa-1} \in \mathcal{C}_{\mathrm{per}}$, find $\phi^{\kappa+1}, \mu^{\kappa+\frac{1}{2}}, \omega^{\kappa+\frac{1}{2}} \in \mathcal{C}_{\mathrm{per}}$ such that

$$\begin{aligned}&\frac{\phi^{\kappa+1} - \phi^\kappa}{\tau} = \Delta_h\mu^{\kappa+\frac{1}{2}},\\ &\mu^{\kappa+\frac{1}{2}} := \chi\left(\phi^\kappa, \phi^{\kappa+1}\right) + (1-\varepsilon)\phi^{\kappa+\frac{1}{2}} + \Delta_h\tilde{\phi}^{\kappa+\frac{1}{2}} + \Delta_h\omega^{\kappa+\frac{1}{2}},\\ &\omega^{\kappa+\frac{1}{2}} := \Delta_h\phi^{\kappa+\frac{1}{2}},\end{aligned} \tag{3.1}$$

where $\phi^0 := \Phi^0$, $\phi^1 := \Phi^1$,

$$\phi^{\kappa+\frac{1}{2}} := \frac{1}{2}\left(\phi^{\kappa+1} + \phi^\kappa\right), \qquad \tilde{\phi}^{\kappa+\frac{1}{2}} := \frac{3}{2}\phi^\kappa - \frac{1}{2}\phi^{\kappa-1}, \quad \text{and} \quad \chi(\phi,\psi) := \frac{1}{4}(\phi+\psi)\left(\phi^2+\psi^2\right).$$

A direct application of the Crank–Nicolson/trapezoidal discretization is made to ω, while the chemical potential, μ, is approximated using several different second-order temporal stencils. Our careful treatment facilitates the energy stability and solvability analyses, which can be found in the following result from [21]:

Proposition 3.1. *Suppose that the exact solution ϕ_e is periodic and sufficiently regular, and $\phi^0, \phi^1 \in \mathcal{C}_{\text{per}}$ is obtained via grid projection, as defined above. For each $1 \le \kappa \le N_t - 1$, there is a unique solution $\phi^{\kappa+1} \in \mathcal{C}_{\text{per}}$ to the scheme (3.1). Furthermore, the scheme (3.1), with starting values ϕ^0 and ϕ^1, is unconditionally energy stable in the following sense: for any $\tau > 0$ and $h > 0$, and any positive integer $2 \le \kappa \le N_t$,*

$$F_h(\phi^\kappa) \le F_h(\phi^1) + \frac{1}{2}\|\nabla_h(\phi^1 - \phi^0)\|_2^2 \le C_0, \tag{3.2}$$

where $C_0 > 0$ is independent of h, τ, ε and T.

Remark 3.2. In the earlier work [21], the energy stability is based on a "ghost" point initial data assumption: $\phi^{-1} = \phi^0$. Under such an assumption, the energy stability result turns out to be simpler, and the addition correction term appearing in (3.2), $\frac{1}{2}\|\nabla_h(\phi^1 - \phi^0)\|_2^2$, does not appear. In this article, we make an alternative assumption: $\phi^0 := \Phi^0$, $\phi^1 := \Phi^1$, which in turn leads to the $O(\tau^2)$ numerical correction term. Meanwhile, such an additional term still assures a uniform in time energy bound, since both ϕ^1 and ϕ^0 are given initial data.

On the other hand, with the "ghost" point initial data assumption as presented in [21], a theoretical justification of the second order temporal accuracy is not obvious, since $\phi^{-1} = \phi^0$ is only an $O(\tau)$ approximation to ϕ^{-1}. Such a theoretical puzzle could be explained as follows. Although the "ghost" extrapolation formula $\phi^{-1} = \phi^0$ is only first order accurate in time, the corresponding numerical solution for ϕ^1 is still second order accurate, due to the subtle fact that, a first order accurate approximation for the right hand side, combined with the temporal discretization $\frac{\phi^1 - \phi^0}{\tau}$, yields a second order accurate ϕ^1. In other words, a first order numerical scheme in the first time step results in a second order accurate solution for ϕ^1. After an $O(\tau^2)$ accurate solution for ϕ^1 is obtained, the numerical algorithm at all the subsequent time steps has the $O(\tau^2)$ temporal truncation error, so that a second order accuracy in time is formally assured.

In this article, the alternative initial data we use: $\phi^0 := \Phi^0$, $\phi^1 := \Phi^1$, avoid the above complicated argument, so that this approach is expected to simplify the convergence analysis in later sections.

Remark 3.3. In the standard PFC model, the parameter ε is set to be $0 \le \varepsilon \le 1$, so that the energy $\frac{1-\varepsilon}{2}\|\phi\|^2$ is convex in the expansion of (1.1); most practical physical cases have also supported such an assumption. On the other hand, even if in the case of $\varepsilon > 1$, the corresponding energy functional $\frac{1-\varepsilon}{2}\|\phi\|^2$ becomes concave, we are still able to treat the associated chemical potential in an explicit way, namely to replace $\phi^{\kappa+1/2}$ by $\tilde{\phi}^{\kappa+1/2} = \frac{3}{2}\phi^k - \frac{1}{2}\phi^{k-1}$, to ensure the energy stability.

The $\|\cdot\|_\infty$ bound of a grid function could be controlled with the help of a discrete Sobolev inequality, as stated by the following theorem; its proof will be given in Section 4.

Theorem 3.4. *Let $\phi \in \mathcal{C}_{\text{per}}$. Then there exists a constant C independent of τ or h such that*

$$\|\phi\|_\infty \le C\|\phi\|_{2,2}. \tag{3.3}$$

As a combination of Proposition 3.1, Theorem 3.4 and inequality (2.4) in Lemma 2.3, the following $\|\cdot\|_\infty$ estimate for the numerical solution is available.

Corollary 3.5. *For the numerical scheme (3.1), we have*

$$\|\phi^\kappa\|_\infty \le C\left(C_0 + \frac{L^3}{4}\right) := \tilde{C}_0, \quad \forall \kappa \ge 0. \tag{3.4}$$

The main theoretical result is stated in the following theorem. Its proof will be given in Section 4.

Theorem 3.6. *Suppose the unique solution ϕ_e for the three-dimensional PFC equation (1.2), with $M(\phi) \equiv 1$, is of regularity class*

$$\phi_e \in \mathcal{R} := H^3(0, T; C^0_{\text{per}}) \cap H^2(0, T; C^4_{\text{per}}) \cap L^\infty(0, T; C^8_{\text{per}}), \tag{3.5}$$

and the initial data $\phi^0, \phi^1 \in \mathcal{C}_{\text{per}}$ are defined as above. Define $e^\kappa_{ijk} := \Phi^\kappa_{ijk} - \phi^\kappa_{ijk}$. Then, provided τ and h are sufficiently small, for all positive integers κ, such that $\tau \cdot \kappa \le T$, we have

$$\|e^\kappa\|_2 \le \hat{C}(h^2 + \tau^2), \tag{3.6}$$

for some $\hat{C} > 0$ that is independent of h and τ.

4. The detailed convergence analysis

4.1. The proof of Theorem 3.4

We begin with the proof of Theorem 3.4, which provides a tool to bound the $\|\cdot\|_\infty$ norm of a grid function in terms of its discrete $\|\cdot\|_{2,2}$ norm.

Proof. For a function $\phi \in \mathcal{C}_{\text{per}}$ with value ϕ_{ijk} at (ξ_i, ξ_j, ξ_k), the IDFT is given by [43]:

$$\phi_{ijk} = \sum_{r,s,t=-R}^{R} \hat{\phi}_{rst} \mathrm{e}^{2\pi i(r\xi_i + s\xi_j + t\xi_k)/L}, \quad i, j, k = 1, \ldots, m, \tag{4.1}$$

where $\hat{\phi}$ is the DFT of ϕ, and, for simplicity of writing, where we have assumed that m is odd: $m = 2R+1$. The corresponding interpolation function is defined as

$$\phi_F(x, y, z) = \sum_{r,s,t=-R}^{R} \hat{\phi}_{rst} \mathrm{e}^{2\pi i(rx+sy+tz)/L}.$$

Using the Parseval's identity (at both the discrete and continuous levels), we have

$$\begin{aligned}
\|\phi\|_2^2 = \|\phi_F\|_{L^2}^2 &= L^3 \sum_{r,s,t=-R}^{R} \left|\hat{\phi}_{rst}\right|^2, \\
D_x\phi_{i+\frac{1}{2},j,k} &= \frac{1}{h}(\phi_{i+1,j,k} - \phi_{i,j,k}) \\
&= \frac{1}{h} \sum_{r,s,t=-R}^{R} \hat{\phi}_{rst} \left[\mathrm{e}^{2\pi i(r\xi_{i+1} + s\xi_j + t\xi_k)/L} - \mathrm{e}^{2\pi i(r\xi_i + s\xi_j + t\xi_k)/L}\right] \\
&= \frac{1}{h} \sum_{r,s,t=-R}^{R} \hat{\phi}_{rst} \mathrm{e}^{2\pi i\left(r\xi_{i+\frac{1}{2}} + s\xi_j + t\xi_k\right)/L} \cdot 2i \sin\frac{\pi rh}{L} \\
&= \sum_{r,s,t=-R}^{R} u_r \hat{\phi}_{rst} \mathrm{e}^{2\pi i\left(r\xi_{i+\frac{1}{2}} + s\xi_j + t\xi_k\right)/L}, \\
\partial_x\phi_F(x, y, z) &= \sum_{r,s,t=-R}^{R} v_r \hat{\phi}_{rst} \mathrm{e}^{2\pi i(rx+sy+tz)/L},
\end{aligned}$$

with

$$u_r = \frac{2i \sin\frac{\pi rh}{L}}{h}, \qquad v_r = \frac{2i\pi r}{L}.$$

A comparison of Fourier eigenvalues between $|u_r|$ and $|v_r|$ shows that

$$\begin{aligned}
&\frac{2}{\pi}|v_r| \le |u_r| \le |v_r|, \quad -R \le r \le R, \\
&[D_x\phi, D_x\phi]_x = h^3 \sum_{i,j,k=1}^{m} \left|D_x\phi_{i+\frac{1}{2},j,k}\right|^2 = L^3 \sum_{r,s,t=-R}^{R} |u_r|^2 |\hat{\phi}_{rst}|^2, \\
&\|\partial_x\phi_F\|^2 = L^3 \sum_{r,s,t=-R}^{R} |v_r|^2 |\hat{\phi}_{rst}|^2.
\end{aligned}$$

Then we get

$$\|\partial_x\phi_F\|^2 = \left|\frac{v_r}{u_r}\right|^2 [D_x\phi, D_x\phi]_x \le \left(\frac{\pi}{2}\right)^2 [D_x\phi, D_x\phi]_x.$$

Similarly, the following estimates are available:

$$\begin{aligned}
&\|\partial_y\phi_F\|^2 \le \left(\frac{\pi}{2}\right)^2 [D_y\phi, D_y\phi]_y, \\
&\|\partial_z\phi_F\|^2 \le \left(\frac{\pi}{2}\right)^2 [D_z\phi, D_z\phi]_z.
\end{aligned}$$

For the second order derivatives, the following estimates are valid:

$$\begin{aligned} d_x(D_x\phi)_{i,j,k} &= \frac{1}{h}\left(D_x\phi_{i+\frac{1}{2},j,k} - D_x\phi_{i-\frac{1}{2},j,k}\right) \\ &= \frac{1}{h}\left(\sum_{r,s,t=-R}^{R} u_r\hat{\phi}_{rst}\mathrm{e}^{2\pi i\left(r\xi_{i+\frac{1}{2}}+s\xi_j+t\xi_k\right)/L} - \sum_{r,s,t=-R}^{R} u_r\hat{\phi}_{rst}\mathrm{e}^{2\pi i\left(r\xi_{i-\frac{1}{2}}+s\xi_j+t\xi_k\right)/L}\right) \\ &= \sum_{r,s,t=-R}^{R} u_r^2\hat{\phi}_{rst}\mathrm{e}^{2\pi i(r\xi_i+s\xi_j+t\xi_k)/L}, \end{aligned}$$

$$\partial_x^2\phi_F(x,y,z) = \sum_{r,s,t=-R}^{R} v_r^2\hat{\phi}_{rst}\mathrm{e}^{2\pi i(rx+sy+tz)/L}.$$

As a consequence, these inequalities yield the following result:

$$\|\partial_x^2\phi_F\|^2 = \left|\frac{v_r}{u_r}\right|^4 \|d_x(D_x\phi)\|_2^2 \le \left(\frac{\pi}{2}\right)^4 \|d_x(D_x\phi)\|_2^2.$$

Similarly,

$$\|\partial_y^2\phi_F\|^2 \le \left(\frac{\pi}{2}\right)^4 \|d_y(D_y\phi)\|_2^2, \qquad \|\partial_z^2\phi_F\|^2 \le \left(\frac{\pi}{2}\right)^4 \|d_z(D_z\phi)\|_2^2,$$

and

$$\begin{aligned} \|\partial_x\partial_y\phi_F\|^2 &\le \frac{1}{2}(\|\partial_x^2\phi_F\|^2 + \|\partial_y^2\phi_F\|^2), \\ \|\partial_x\partial_z\phi_F\|^2 &\le \frac{1}{2}(\|\partial_x^2\phi_F\|^2 + \|\partial_z^2\phi_F\|^2), \\ \|\partial_y\partial_z\phi_F\|^2 &\le \frac{1}{2}(\|\partial_y^2\phi_F\|^2 + \|\partial_z^2\phi_F\|^2). \end{aligned}$$

Then we arrive at

$$\begin{aligned} \|\phi_F\|_{H^2}^2 &= |\phi_F|_{0,2}^2 + |\phi_F|_{1,2}^2 + |\phi_F|_{2,2}^2 \\ &\le \|\phi_F\|^2 + \|\partial_x\phi_F\|^2 + \|\partial_y\phi_F\|^2 + \|\partial_z\phi_F\|^2 + 2(\|\partial_x^2\phi_F\|^2 + \|\partial_y^2\phi_F\|^2 + \|\partial_z^2\phi_F\|^2) \\ &\le \|\phi\|_2^2 + \left(\frac{\pi}{2}\right)^2 \left([D_x\phi, D_x\phi]_x + [D_y\phi, D_y\phi]_y + [D_z\phi, D_z\phi]_z\right) \\ &\quad + 2\times\left(\frac{\pi}{2}\right)^4 \left(\|d_x(D_x\phi)\|_2^2 + \|d_y(D_y\phi)\|_2^2 + \|d_z(D_z\phi)\|_2^2\right) \\ &= \|\phi\|_2^2 + \left(\frac{\pi}{2}\right)^2 \|\nabla_h\phi\|_2^2 + 2\times\left(\frac{\pi}{2}\right)^4 \|\Delta_h\phi\|_2^2 \\ &\le 2\cdot\left(\frac{\pi}{2}\right)^4 (\|\phi\|_2^2 + \|\nabla_h\phi\|_2^2 + \|\Delta_h\phi\|_2^2) \\ &= 2\cdot\left(\frac{\pi}{2}\right)^4 \|\phi\|_{2,2}^2. \end{aligned}$$

Meanwhile, since ϕ is the discrete interpolant of the continuous function, we observe that $\|\phi\|_\infty \le \|\phi_F\|_{L^\infty}$, which implies the following estimate:

$$\|\phi\|_\infty \le \|\phi_F\|_{L^\infty} \le C_1\|\phi_F\|_{H^2} \le \frac{\sqrt{2}\pi^2}{4}C_1\|\phi\|_{2,2},$$

which gives (3.3). This completes the proof of Theorem 3.4. ■

4.2. The proof of Theorem 3.6

Corollary 3.5 is a direct consequence of Theorem 3.4, so that a uniform in time $\|\cdot\|_\infty$ bound of the numerical solution becomes available. With the help of the bound (3.4), we proceed into the convergence proof in Theorem 3.6.

Proof. An application of the Taylor expansion for the exact solution ϕ_e at $(\xi_i, \xi_j, \xi_k, t_{\kappa+\frac{1}{2}})$ implies that

$$\begin{aligned}
&\frac{\Phi_{ijk}^{\kappa+1}-\Phi_{ijk}^{\kappa}}{\tau}=\Delta_h U_{ijk}^{\kappa+\frac{1}{2}}+R_{ijk}^{\kappa},\quad 1\le i\le m,\quad 1\le j\le n,\quad 1\le k\le l,\quad 2\le\kappa\le N_t,\\
&U_{ijk}^{\kappa+\frac{1}{2}}=(\Phi_{ijk}^{\kappa+\frac{1}{2}})(\Phi_{ijk}^{2})^{\kappa+\frac{1}{2}}+(1-\varepsilon)\Phi_{ijk}^{\kappa+\frac{1}{2}}+3\Delta_h\Phi_{ijk}^{\kappa}-\Delta_h\Phi_{ijk}^{\kappa-1}+\Delta_h(\Delta_h\Phi_{ijk})^{\kappa+\frac{1}{2}}+S_{ijk}^{\kappa},\\
&\quad 1\le i\le m,\quad 1\le j\le n,\quad 1\le k\le l,\quad 2\le\kappa\le N_t,\\
&\Phi_{ijk}^{0}=\psi(\xi_i,\xi_j,\xi_k)\quad 1\le i\le m,\quad 1\le j\le n,\quad 2\le k\le l,
\end{aligned}\tag{4.2}$$

in which the local truncation errors R_{ijk}^{κ} and S_{ijk}^{κ} satisfy

$$|R_{ijk}^{\kappa}|\le C_3(\tau^2+h^2),\qquad |S_{ijk}^{\kappa}|\le C_3(\tau^2+h^2),\quad 1\le i\le m,\ 1\le j\le n,\ 1\le k\le l,\ 2\le\kappa\le N_t,\tag{4.3}$$

for some $C_3\ge 0$, dependent only on T and L.

To facilitate the convergence analysis, we denote

$$C_4=\|\Phi\|_{L^\infty(0,T;\Omega)}.\tag{4.4}$$

The uniform in time $\|\cdot\|_\infty$ bound for the numerical solution is given by $\tilde{C}_0$, as defined as (3.4). These two bounds will be useful in the nonlinear error estimate.

Subtracting (3.1) from (4.2) leads to the following error evolutionary equation:

$$\begin{aligned}
\frac{e^{\kappa+1}-e^{\kappa}}{\tau}=\ &\Delta_h\left\{\left[\left(\Phi^{\kappa+\frac{1}{2}}\right)(\Phi^2)^{\kappa+\frac{1}{2}}-\left(\phi^{\kappa+\frac{1}{2}}\right)(\phi^2)^{\kappa+\frac{1}{2}}\right]+(1-\varepsilon)e^{\kappa+\frac{1}{2}}\right.\\
&\left.+(3\Delta_h e^{\kappa}-\Delta_h e^{\kappa-1})+\Delta_h(\Delta_h e)^{\kappa+\frac{1}{2}}+S^{\kappa}\right\}+R^{\kappa}.
\end{aligned}\tag{4.5}$$

Taking a discrete inner product with (4.5) by $e^{\kappa+\frac{1}{2}}$, we get

$$\begin{aligned}
\left(\frac{e^{\kappa+1}-e^{\kappa}}{\tau},e^{\kappa+\frac{1}{2}}\right)=\ &\left(\Phi^{\kappa+\frac{1}{2}}(\Phi^2)^{\kappa+\frac{1}{2}}-\phi^{\kappa+\frac{1}{2}}(\phi^2)^{\kappa+\frac{1}{2}},\Delta_h e^{\kappa+\frac{1}{2}}\right)+(1-\varepsilon)\left(\Delta_h e^{\kappa+\frac{1}{2}},e^{\kappa+\frac{1}{2}}\right)\\
&+\left(\Delta_h(3\Delta_h e^{\kappa}-\Delta_h e^{\kappa-1}),e^{\kappa+\frac{1}{2}}\right)+\left(\Delta_h^3 e^{\kappa+\frac{1}{2}},e^{\kappa+\frac{1}{2}}\right)\\
&+\left(\Delta_h S^{\kappa},e^{\kappa+\frac{1}{2}}\right)+\left(R^{\kappa},e^{\kappa+\frac{1}{2}}\right).
\end{aligned}\tag{4.6}$$

For the left hand side of (4.6), the following identity is valid:

$$\left(\frac{e^{\kappa+1}-e^{\kappa}}{\tau},e^{\kappa+\frac{1}{2}}\right)=\frac{1}{2\tau}(\|e^{\kappa+1}\|_2^2-\|e^{\kappa}\|_2^2).\tag{4.7}$$

For the nonlinear error term on the right hand side of (4.6), we have

$$\begin{aligned}
&\left(\Phi^{\kappa+\frac{1}{2}}(\Phi^2)^{\kappa+\frac{1}{2}}-\phi^{\kappa+\frac{1}{2}}(\phi^2)^{\kappa+\frac{1}{2}},\Delta_h e^{\kappa+\frac{1}{2}}\right)\\
&=\left(\Phi^{\kappa+\frac{1}{2}}\frac{(\Phi^{\kappa})^2+(\Phi^{\kappa+1})^2}{2}-\phi^{\kappa+\frac{1}{2}}\frac{(\phi^{\kappa})^2+(\phi^{\kappa+1})^2}{2},\Delta_h e^{\kappa+\frac{1}{2}}\right)\\
&=\left(\Phi^{\kappa+\frac{1}{2}}\left(\frac{(\Phi^{\kappa+1})^2-(\phi^{\kappa+1})^2}{2}+\frac{(\Phi^{\kappa})^2-(\phi^{\kappa})^2}{2}\right)+\left(\Phi^{\kappa+\frac{1}{2}}-\phi^{\kappa+\frac{1}{2}}\right)\frac{(\phi^{\kappa})^2+(\phi^{\kappa+1})^2}{2},\Delta_h e^{\kappa+\frac{1}{2}}\right)\\
&=\left(\Phi^{\kappa+\frac{1}{2}}\left(\frac{\Phi^{\kappa+1}+\phi^{\kappa+1}}{2}e^{\kappa+1}+\frac{\Phi^{\kappa}+\phi^{\kappa}}{2}e^{\kappa}\right)+\frac{(\phi^{\kappa})^2+(\phi^{\kappa+1})^2}{2}e^{\kappa+\frac{1}{2}},\Delta_h e^{\kappa+\frac{1}{2}}\right)\\
&\le\frac{1}{4}\left[2C_4^2+(C_4+\tilde{C}_0)^2\right](\|e^{\kappa+1}\|_2+\|e^{\kappa}\|_2)\cdot\left\|\Delta_h e^{\kappa+\frac{1}{2}}\right\|_2\\
&\le\frac{1}{2}\left\|\Delta_h e^{\kappa+\frac{1}{2}}\right\|_2^2+C(C_4^4+\tilde{C}_0^4)(\|e^{\kappa+1}\|_2^2+\|e^{\kappa}\|_2^2),
\end{aligned}\tag{4.8}$$

in which the discrete Hölder inequality has been repeatedly applied. The second and fourth terms on the right hand side of (4.6) could be analyzed in a straightforward way:

$$(1-\varepsilon)\left(\Delta_h e^{\kappa+\frac{1}{2}},e^{\kappa+\frac{1}{2}}\right)=-(1-\varepsilon)\left\|\nabla_h e^{\kappa+\frac{1}{2}}\right\|_2^2,\tag{4.9}$$

$$\left(\Delta_h^3 e^{\kappa+\frac{1}{2}},e^{\kappa+\frac{1}{2}}\right)=-\left\|\nabla_h\Delta_h e^{\kappa+\frac{1}{2}}\right\|_2^2.\tag{4.10}$$

For the third term of the right hand side of (4.6), the following estimate is applied:

$$\left(\Delta_h(3\Delta_h e^{\kappa} - \Delta_h e^{\kappa-1}), e^{\kappa+\frac{1}{2}}\right) \tag{4.11}$$

$$= \left(3\Delta_h e^{\kappa} - \Delta_h e^{\kappa-1}, \Delta_h e^{\kappa+\frac{1}{2}}\right) = \left(3\Delta_h e^{\kappa} - \Delta_h\left(2e^{\kappa-\frac{1}{2}} - e^{\kappa}\right), \Delta_h e^{\kappa+\frac{1}{2}}\right) \tag{4.12}$$

$$= \left(4\Delta_h e^{\kappa} - 2\Delta_h e^{\kappa-\frac{1}{2}}, \Delta_h e^{\kappa+\frac{1}{2}}\right) \tag{4.13}$$

$$= \left((2\Delta_h e^{\kappa+1} + 2\Delta_h e^{\kappa}) - (2\Delta_h e^{\kappa+1} - 2\Delta_h e^{\kappa}) - 2\Delta_h e^{\kappa-\frac{1}{2}}, \Delta_h e^{\kappa+\frac{1}{2}}\right) \tag{4.14}$$

$$= 4\left\|\Delta_h e^{\kappa+\frac{1}{2}}\right\|_2^2 - \|\Delta_h e^{\kappa+1}\|_2^2 + \|\Delta_h e^{\kappa}\|_2^2 - 2\left(\Delta_h e^{\kappa-\frac{1}{2}}, \Delta_h e^{\kappa+\frac{1}{2}}\right) \tag{4.15}$$

$$\le 4\left\|\Delta_h e^{\kappa+\frac{1}{2}}\right\|_2^2 - \|\Delta_h e^{\kappa+1}\|_2^2 + \|\Delta_h e^{\kappa}\|_2^2 + \left\|\Delta_h e^{\kappa-\frac{1}{2}}\right\|_2^2 + \left\|\Delta_h e^{\kappa+\frac{1}{2}}\right\|_2^2 \tag{4.16}$$

$$\le 5\left\|\Delta_h e^{\kappa+\frac{1}{2}}\right\|_2^2 + \left\|\Delta_h e^{\kappa-\frac{1}{2}}\right\|_2^2 - \|\Delta_h e^{\kappa+1}\|_2^2 + \|\Delta_h e^{\kappa}\|_2^2. \tag{4.17}$$

The fifth term and sixth terms on the right hand side of (4.6) could be bounded with an application of Cauchy inequality:

$$\left(\Delta_h S^{\kappa}, e^{\kappa+\frac{1}{2}}\right) \le \frac{1}{2}\|S^{\kappa}\|_2^2 + \frac{1}{2}\left\|\Delta_h e^{\kappa+\frac{1}{2}}\right\|_2^2, \tag{4.18}$$

$$\left(R^{\kappa}, e^{\kappa+\frac{1}{2}}\right) \le \frac{1}{2}\|R^{\kappa}\|_2^2 + \frac{1}{2}\left\|e^{\kappa+\frac{1}{2}}\right\|_2^2. \tag{4.19}$$

Therefore, a substitution of (4.7)–(4.18) into (4.6) yields

$$\begin{aligned}
&\frac{1}{2\tau}(\|e^{\kappa+1}\|_2^2 - \|e^{\kappa}\|_2^2) + \left\|\nabla_h\Delta_h e^{\kappa+\frac{1}{2}}\right\|_2^2 + (1-\varepsilon)\left\|\nabla_h e^{\kappa+\frac{1}{2}}\right\|_2^2 \\
&\le C(C_4^4 + \tilde{C}_0^4)(\|e^{\kappa+1}\|_2^2 + \|e^{\kappa}\|_2^2) + \frac{1}{2}\|e^{\kappa+\frac{1}{2}}\|_2^2 + \frac{1}{2}(\|S^{\kappa}\|_2^2 + \|R^{\kappa}\|_2^2) \\
&\quad + 6\left\|\Delta_h e^{\kappa+\frac{1}{2}}\right\|_2^2 + \left\|\Delta_h e^{\kappa-\frac{1}{2}}\right\|_2^2 - \|\Delta_h e^{\kappa+1}\|_2^2 + \|\Delta_h e^{\kappa}\|_2^2 \\
&\le C(C_4^4 + \tilde{C}_0^4 + 1)(\|e^{\kappa+1}\|_2^2 + \|e^{\kappa}\|_2^2) + \frac{1}{2}(\|S^{\kappa}\|_2^2 + \|R^{\kappa}\|_2^2) \\
&\quad + 6\left\|\Delta_h e^{\kappa+\frac{1}{2}}\right\|_2^2 + \left\|\Delta_h e^{\kappa-\frac{1}{2}}\right\|_2^2 - \|\Delta_h e^{\kappa+1}\|_2^2 + \|\Delta_h e^{\kappa}\|_2^2.
\end{aligned} \tag{4.20}$$

By Lemma 2.2, we obtain

$$6\left\|\Delta_h e^{\kappa+\frac{1}{2}}\right\|_2^2 \le 6\left(\frac{12^2}{3}\left\|e^{\kappa+\frac{1}{2}}\right\|_2^2 + \frac{2}{36}\left\|\nabla_h\Delta_h e^{\kappa+\frac{1}{2}}\right\|_2^2\right), \tag{4.21}$$

$$\left\|\Delta_h e^{\kappa-\frac{1}{2}}\right\|_2^2 \le \left(\frac{1^2}{3}\left\|e^{\kappa-\frac{1}{2}}\right\|_2^2 + \frac{2}{3}\left\|\nabla_h\Delta_h e^{\kappa-\frac{1}{2}}\right\|_2^2\right). \tag{4.22}$$

Going back (4.20), we arrive at

$$\begin{aligned}
&\frac{1}{2\tau}(\|e^{\kappa+1}\|_2^2 - \|e^{\kappa}\|_2^2) + \left\|\nabla_h\Delta_h e^{\kappa+\frac{1}{2}}\right\|_2^2 + \|\Delta_h e^{\kappa+1}\|_2^2 - \|\Delta_h e^{\kappa}\|_2^2 \\
&\le 288\left\|e^{\kappa+\frac{1}{2}}\right\|_2^2 + \frac{1}{3}\left\|\nabla_h\Delta_h e^{\kappa+\frac{1}{2}}\right\|_2^2 + \frac{1}{3}\left\|e^{\kappa-\frac{1}{2}}\right\|_2^2 + \frac{2}{3}\left\|\nabla_h\Delta_h e^{\kappa-\frac{1}{2}}\right\|_2^2 \\
&\quad + \frac{1}{2}(\|S^{\kappa}\|_2^2 + \|R^{\kappa}\|_2^2) + C(C_4^4 + \tilde{C}_0^4 + 1)(\|e^{\kappa+1}\|_2^2 + \|e^{\kappa}\|_2^2).
\end{aligned} \tag{4.23}$$

A summation in time implies that

$$\frac{1}{2\tau}(\|e^{\kappa+1}\|_2^2 - \|e^{1}\|_2^2) + \|\Delta_h e^{\kappa+1}\|_2^2 - \|\Delta_h e^{1}\|_2^2 \le \frac{1}{2}\sum_{i=1}^{\kappa}(\|S^i\|_2^2 + \|R^i\|_2^2) + C\sum_{i=0}^{\kappa}(C_4^4 + \tilde{C}_0^4 + 1)\|e^i\|_2^2. \tag{4.24}$$

Note that the constant C appearing on the right hand side of (4.24) is different than that appearing on the right hand side of (4.23), and we have used the fact that $\frac{\frac{1}{2}}{\frac{1}{2}-C(C_4^4+\tilde{C}_0^4+1)\tau} \le \frac{1}{2} + C'(C_4^4 + \tilde{C}_0^4 + 1)\tau$. In turn, an application of discrete Gronwall inequality (cited from [44], stated in Appendix), combined with the local truncation error estimate (4.3), yields the desired

convergence result

$$\begin{aligned}\|e^{\kappa+1}\|_2^2 + 2\tau\|\Delta_h e^{\kappa+1}\|_2^2 &\le \left(\|e^1\|_2^2 + 2\tau\|\Delta_h e^1\|_2^2 + 2C_3^2T(\tau^2+h^2)^2\right)\exp(\tilde{C}t^\kappa)\\ &\le C_3^2(2T+2)\exp(\tilde{C}t^\kappa)(\tau^2+h^2)^2,\end{aligned} \tag{4.25}$$

with $\tilde{C} = C(C_4^4 + \tilde{C}_0^4 + 1)$. Therefore, the convergence estimate (3.6) is valid, for the right hand constant $\hat{C}$ taken as

$$\hat{C} = C_3(2T+2)^{1/2}\exp(\tilde{C}t^\kappa). \tag{4.26}$$

This completes the proof of Theorem 3.6. ■

5. Nonlinear multigrid solvers

In this section we present the details of the nonlinear multigrid method that we use for solving the semi-implicit numerical scheme (3.1). The fully finite-difference scheme (3.1) is formulated as follows: Find $\phi_{i,j,k}^{\kappa+1}$, $\mu_{i,j,k}^{\kappa+1/2}$ and $\omega_{i,j,k}^{\kappa+1/2}$ in $\mathcal{C}_{\text{per}}$ such that

$$\begin{aligned}&\phi_{i,j,k}^{\kappa+1} - \tau d_x\left(M\left(A_x\tilde{\phi}^{\kappa+\frac{1}{2}}\right)D_x\mu^{\kappa+\frac{1}{2}}\right)_{i,j,k}\\ &- \tau d_y\left(M\left(A_y\tilde{\phi}^{\kappa+\frac{1}{2}}\right)D_y\mu^{\kappa+\frac{1}{2}}\right)_{i,j,k} - \tau d_z\left(M\left(A_z\tilde{\phi}^{\kappa+\frac{1}{2}}\right)D_z\mu^{\kappa+\frac{1}{2}}\right)_{i,j,k} = \phi_{i,j,k}^{\kappa},\end{aligned} \tag{5.1}$$

$$\begin{aligned}\mu_{i,j,k}^{\kappa+\frac{1}{2}} &- \frac{1}{4}\left(\phi_{i,j,k}^{\kappa+1}+\phi_{i,j,k}^{\kappa}\right)\left((\phi_{i,j,k}^{\kappa+1})^2+(\phi_{i,j,k}^{\kappa})^2\right) - \frac{1-\varepsilon}{2}\left(\phi_{i,j,k}^{\kappa+1}+\phi_{i,j,k}^{\kappa}\right)\\ &- 3\Delta_h\phi_{i,j,k}^{\kappa} + \Delta_h\phi_{i,j,k}^{\kappa-1} - \Delta_h\omega_{i,j,k}^{\kappa+\frac{1}{2}} = 0,\end{aligned} \tag{5.2}$$

$$\omega_{i,j,k}^{\kappa+\frac{1}{2}} - \frac{1}{2}\left(\Delta_h\phi_{i,j,k}^{\kappa+1} + \Delta_h\phi_{i,j,k}^{\kappa}\right) = 0, \tag{5.3}$$

where $\tilde{\phi}^{\kappa+\frac{1}{2}} = \frac{3}{2}\phi^{\kappa} - \frac{1}{2}\phi^{\kappa-1}$. Denote $\mathbf{u} = (\phi_{i,j,k}^{\kappa+1}, \mu_{i,j,k}^{\kappa+1/2}, \omega_{i,j,k}^{\kappa+1/2})^T$. Then the above discrete nonlinear system can be written in terms of a nonlinear operator $\mathbf{N}$ and source term $\mathbf{S}$ such that

$$\mathbf{N}(\mathbf{u}) = \mathbf{S}. \tag{5.4}$$

The $3\times m\times n\times l$ nonlinear operator $\mathbf{N}(\mathbf{u}^{\kappa+1}) = \left(N_{i,j,k}^{(1)}(\mathbf{u}), N_{i,j,k}^{(2)}(\mathbf{u}), N_{i,j,k}^{(3)}(\mathbf{u})\right)^T$ can be defined as

$$\begin{aligned}N_{i,j,k}^{(1)}(\mathbf{u}) = \phi_{i,j,k}^{\kappa+1} &- \tau d_x\left(M\left(A_x\tilde{\phi}^{\kappa+\frac{1}{2}}\right)D_x\mu^{\kappa+\frac{1}{2}}\right)_{i,j,k} - \tau d_y\left(M\left(A_y\tilde{\phi}^{\kappa+\frac{1}{2}}\right)D_y\mu^{\kappa+\frac{1}{2}}\right)_{i,j,k}\\ &- \tau d_z\left(M\left(A_z\tilde{\phi}^{\kappa+\frac{1}{2}}\right)D_z\mu^{\kappa+\frac{1}{2}}\right)_{i,j,k},\end{aligned} \tag{5.5}$$

$$N_{i,j,k}^{(2)}(\mathbf{u}) = \mu_{i,j,k}^{\kappa+\frac{1}{2}} - \frac{1}{4}\left(\phi_{i,j,k}^{\kappa+1}+\phi_{i,j,k}^{\kappa}\right)\left((\phi_{i,j,k}^{\kappa+1})^2+(\phi_{i,j,k}^{\kappa})^2\right) - \frac{1-\varepsilon}{2}\phi_{i,j,k}^{\kappa+1} - \Delta_h\omega_{i,j,k}^{\kappa+\frac{1}{2}}, \tag{5.6}$$

$$N_{i,j,k}^{(3)}(\mathbf{u}) = \omega_{i,j,k}^{\kappa+\frac{1}{2}} - \frac{1}{2}\Delta_h\phi_{i,j,k}^{\kappa+1}, \tag{5.7}$$

and the $3\times m\times n\times l$ source $\mathbf{S} = \left(S_{i,j,k}^{(1)}, S_{i,j,k}^{(2)}, S_{i,j,k}^{(3)}\right)^T$ is given by

$$S_{i,j,k}^{(1)} = \phi_{i,j,k}^{\kappa}, \tag{5.8}$$

$$S_{i,j,k}^{(2)} = \frac{1-\varepsilon}{2}\phi_{i,j,k}^{\kappa} + 3\Delta_h\phi_{i,j,k}^{\kappa} - \Delta_h\phi_{i,j,k}^{\kappa-1}, \tag{5.9}$$

$$S_{i,j,k}^{(3)} = \frac{1}{2}\Delta_h\phi_{i,j,k}^{\kappa}. \tag{5.10}$$

The system (5.4) can be efficiently solved using a nonlinear Full Approximation Scheme (FAS) multigrid method (Algorithm 1: ν_1 and ν_2 are pre-smoothing and post-smoothing steps, ℓ, L are the current level and coarsest levels, and $\mathbf{I}_\ell^{\ell+1}$, $\mathbf{I}_{\ell+1}^{\ell}$ are coarsening and interpolating operators, respectively). More details can be found in [45]. Since we are using a standard FAS V-cycle approach, as reported in earlier works [21,22,35,42,46], we only provide the details of nonlinear smoothing scheme. For smoothing operator, we use a nonlinear Gauss–Seidel method with Red–Black ordering.

Let n be the smoothing iteration, and define

$$M_{i+\frac{1}{2},j,k}^{x} := M\left(\frac{1}{2}A_x\phi_{i+\frac{1}{2},j,k}^{\kappa} - \frac{1}{2}A_x\phi_{i+\frac{1}{2},j,k}^{\kappa-1}\right),$$

$$M_{i,j+\frac{1}{2},k}^{y} := M\left(\frac{1}{2}A_y\phi_{i,j+\frac{1}{2},k}^{\kappa} - \frac{1}{2}A_y\phi_{i,j+\frac{1}{2},k}^{\kappa-1}\right),$$

$$M_{i,j,k+\frac{1}{2}}^{z} := M\left(\frac{1}{2}A_z\phi_{i,j,k+\frac{1}{2}}^{\kappa} - \frac{1}{2}A_z\phi_{i,j,k+\frac{1}{2}}^{\kappa-1}\right).$$

Algorithm 1 Nonlinear Multigrid Method (FAS)

```
Given u^0
procedure FAS(N^0, u^0, S^0, ν1, ν2, ℓ = 0)
    while residual > tolerance do
        Pre-smooth: u^ℓ :=smooth(N^ℓ, u^ℓ, S^ℓ, ν1)            ▷ nonlinear Gauss–Seidel method
        Residual: r^ℓ = S^ℓ − N^ℓ u^ℓ
        Coarsening: r^{ℓ+1} = I_ℓ^{ℓ+1} r^ℓ, u^{ℓ+1} = I_ℓ^{ℓ+1} u^ℓ
        if ℓ = L then
            Solve: N^{ℓ+1} v^{ℓ+1} = N^{ℓ+1} u^{ℓ+1} + r^{ℓ+1}   ▷ Cramer's rule
            Error: e^{ℓ+1} = v^{ℓ+1} − u^{ℓ+1}
        else
            Recursion: FAS(N^{ℓ+1}, u^{ℓ+1}, S^{ℓ+1}, ν1, ν2, ℓ + 1)
        end if
        Correction: u^ℓ = u^ℓ + I_{ℓ+1}^ℓ e^{ℓ+1}
        Post-smooth: u^ℓ :=smooth(N^ℓ, u^ℓ, S^ℓ, ν2)           ▷ nonlinear Gauss–Seidel method
    end while
end procedure
```

Then the smoothing scheme is given by: for every (i, j, k), stepping lexicographically from $(1, 1, 1)$ to (m, n, l), find $\phi_{i,j,k}^{\kappa+1,n+1}$, $\mu_{i,j,k}^{\kappa+\frac{1}{2},n+1}$, $\kappa_{i,j,k}^{\kappa+\frac{1}{2},n+1}$ that solve the 3×3 linear system

$$\begin{aligned}
\phi_{i,j,k}^{\kappa+1,n+1} + \frac{\tau}{h^2}\left(M^x_{i+\frac{1}{2},j,k} + M^x_{i-\frac{1}{2},j,k} + M^y_{i,j+\frac{1}{2},k} + M^y_{i,j-\frac{1}{2},k} + M^z_{i,j,k+\frac{1}{2}} + M^z_{i,j,k-\frac{1}{2}}\right)\mu_{i,j,k}^{\kappa+\frac{1}{2},n+1} &= \tilde{S}^{(1)}_{i,j,k},\\
\mu_{i,j,k}^{\kappa+\frac{1}{2},n+1} - \left(\frac{1}{4}\left((\phi_{i,j,k}^{\kappa+1,n})^2 + (\phi_{i,j,k}^{\kappa})^2\right) + \frac{1-\varepsilon}{2}\right)\phi_{i,j,k}^{k+1,n+1} + \frac{6}{h^2}\omega_{i,j,k}^{\kappa+\frac{1}{2},n+1} &= \tilde{S}^{(2)}_{i,j,k},\\
\omega_{i,j,k}^{\kappa+\frac{1}{2}} + \frac{3}{h^2}\phi_{i,j,k}^{\kappa+1,n+1} &= \tilde{S}^{(3)}_{i,j,k},
\end{aligned}$$

where

$$\begin{aligned}
\tilde{S}^{(1)}_{i,j,k} &:= S^{(1)}_{i,j,k} + \frac{\tau}{h^2}\left(M^x_{i+\frac{1}{2},j,k}\mu_{i+1,j,k}^{\kappa+\frac{1}{2},n} + M^x_{i-\frac{1}{2},j,k}\mu_{i-1,j,k}^{\kappa+\frac{1}{2},n+1} + M^y_{i,j+\frac{1}{2},k}\mu_{i,j+1,k}^{\kappa+\frac{1}{2},n} + M^y_{i,j-\frac{1}{2},k}\mu_{i,j-1,k}^{\kappa+\frac{1}{2},n+1}\right.\\
&\quad \left. + M^z_{i,j,k+\frac{1}{2}}\mu_{i,j,k+1}^{\kappa+\frac{1}{2},n} + M^z_{i,j,k-\frac{1}{2}}\mu_{i,j,k-1}^{\kappa+\frac{1}{2},n+1}\right),\\
\tilde{S}^{(2)}_{i,j,k} &:= S^{(2)}_{i,j,k} + \frac{1}{4}\left((\phi_{i,j,k}^{\kappa+1,n})^2 + (\phi_{i,j,k}^{k})^2\right)\phi_{i,j,k}^{k}\\
&\quad + \frac{1}{h^2}\left(\omega_{i+1,j,k}^{\kappa+\frac{1}{2},n} + \omega_{i-1,j,k}^{\kappa+\frac{1}{2},n+1} + \omega_{i,j+1,k}^{\kappa+\frac{1}{2},n} + \omega_{i,j-1,k}^{\kappa+\frac{1}{2},n+1} + \omega_{i,j,k+1}^{\kappa+\frac{1}{2},n} + \omega_{i,j,k-1}^{\kappa+\frac{1}{2},n+1}\right),\\
\tilde{S}^{(3)}_{i,j,k} &:= S^{(3)}_{i,j,k} + \frac{1}{2h^2}\left(\phi_{i+1,j,k}^{\kappa+1,n} + \phi_{i-1,j,k}^{\kappa+1,n+1} + \phi_{i,j+1,k}^{\kappa+1,n} + \phi_{i,j-1,k}^{\kappa+1,n+1} + \phi_{i,j,k+1}^{\kappa+1,n} + \phi_{i,j,k-1}^{\kappa+1,n+1}\right).
\end{aligned}$$

The above linearized system, which comes from a local Picard linearization of the cubic term in the Gauss–Seidel scheme, can be solved by Cramer's Rule.

6. Numerical results

In this section, we perform some numerical simulations for the three-dimensional scheme (3.1), to verify the theoretical results.

6.1. Convergence and complexity of the multigrid solver

In this subsection we demonstrate the accuracy and efficiency of the multigrid solver. We present the results of the convergence tests and perform some sample computations to verify the convergence and near optimal complexity with respect to the grid size h.

In the first part of this test, we demonstrate the second order accuracy in time and space. The initial data is given by

$$\phi_0(x, y, z) = 0.2 + 0.05\cos\big(2\pi x/3.2\big)\cos\big(2\pi y/3.2\big)\cos\big(2\pi z/3.2\big), \tag{6.1}$$

with $\Omega = [0, 3.2]^3$, $\varepsilon = 2.5 \times 10^{-2}$, $\tau = 0.05h$ and $T = 0.16$. We use a linear refinement path, *i.e.*, $\tau = Ch$. At the final time $T = 0.16$, we expect the global error to be $\mathcal{O}(\tau^2) + \mathcal{O}(h^2) = \mathcal{O}(h^2)$ under either the ℓ^2 or ℓ^∞ norm, as $h, \tau \to 0$. Since we

Table 1
Average CPU time for each time iteration (relatively fine grid), errors and convergence rates. Parameters are given in the text, and the initial data are defined in (6.1). The refinement path is $\tau = 0.05h$. The grid sizes indicate the relatively coarse-fine grid sizes.

Grid sizes	$16^3 - 32^3$	$32^3 - 64^3$	$64^3 - 128^3$
CPU (s)	0.5744	1.5149	8.8971
Error	2.3371×10^{-8}	5.8027×10^{-9}	1.4411×10^{-9}
Rate	–	2.0099	2.0096

Table 2
The number of multigrid iterations of each residual below the tolerance $tol = 10^{-8}$ at the 10-th time step (i.e. at time 1.0×10^{-2} with time steps $\tau = 1.0 \times 10^{-3}$), The rest of parameters are $\varepsilon = 2.5 \times 10^{-2}$, and $\Omega = [0, 3.2] \times [0, 3.2] \times [0, 3.2]$.

(ν_1, ν_2)	Grid sizes			
	16	32	64	128
(1, 1)	7	9	12	21
(2, 2)	4	5	5	5

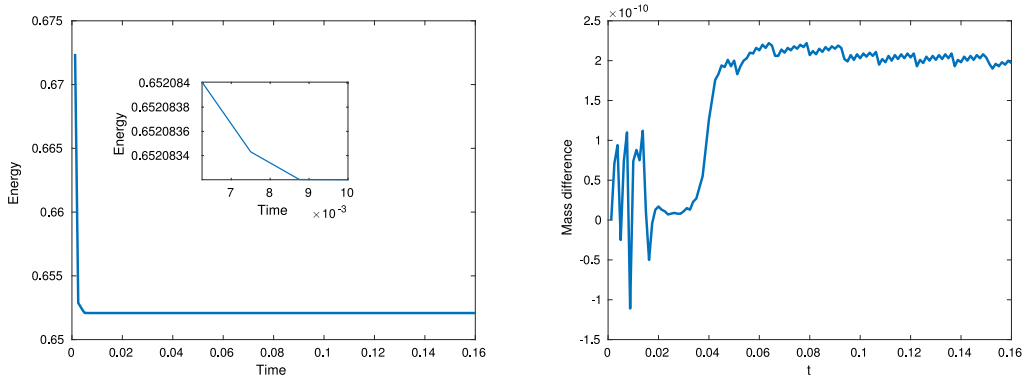

(a) The energy decay. (b) Mass conservation.

Fig. 1. The plots of energy decay and mass conservation. The rest of parameters are $\Omega = [0, 3.2]^3$, $h = 3.2/128$, $\varepsilon = 2.5 \times 10^{-2}$, $\tau = 0.05h$ and $T = 0.16$ and the initial condition is (6.1).

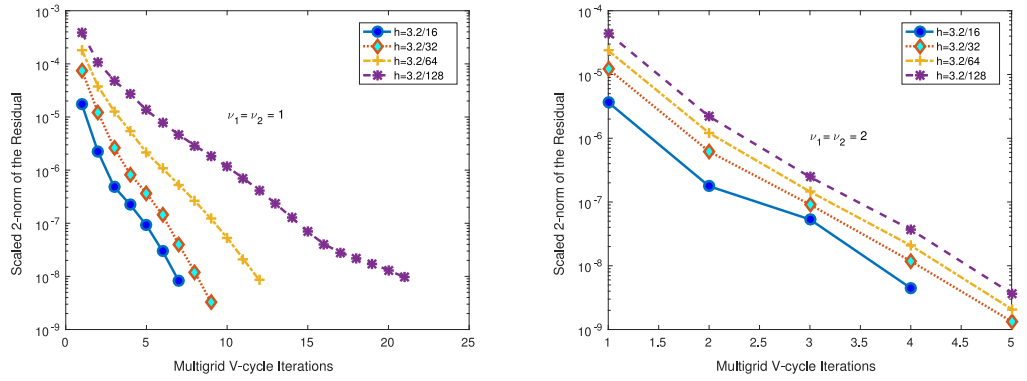

(a) $\nu_1 = \nu_2 = 1$. (b) $\nu_1 = \nu_2 = 2$.

Fig. 2. The reduction in the norm of the residual for each V-cycle iteration at the 10th time step (i.e. at time 1.0×10^{-1} with time steps $\tau = 1.0 \times 10^{-3}$). The rest of parameters are $\varepsilon = 5.0 \times 10^{-2}$, and $\Omega = [0, 3.2] \times [0, 3.2] \times [0, 3.2]$ and the initial condition is (6.1).

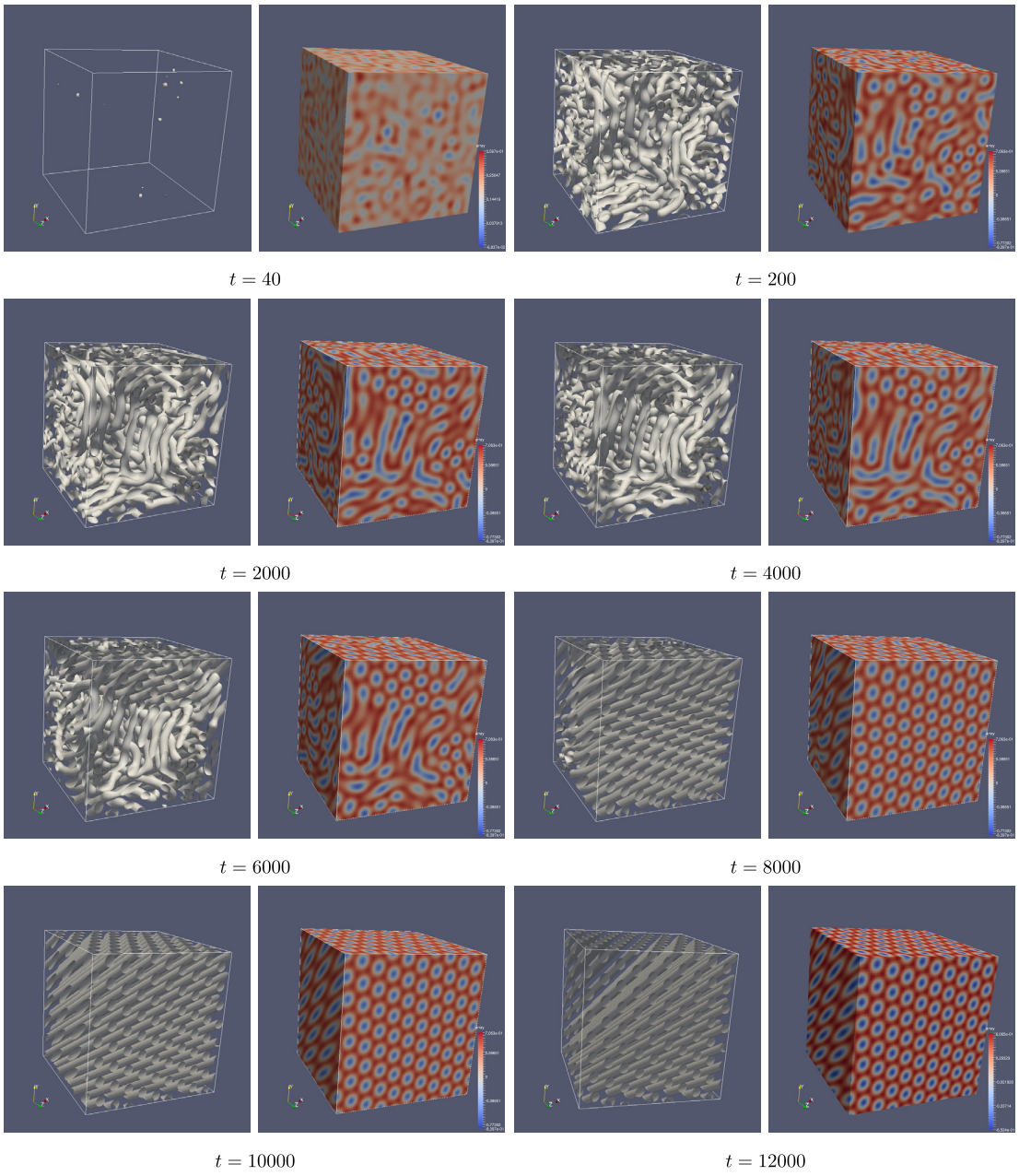

Fig. 3. Three-dimensional periodic micro-structures snapshots with initial condition (6.2) at $t = 40, 200, 2000, 4000, 6000, 8000, 10\,000$ and $12\,000$. Left: iso-surface plots of $\phi = 0.0$, Right: snapshots of micro-structures plots. The parameters are $\varepsilon = 2.5 \times 10^{-1}$, $h = 64/64 = 1.0$, $\Omega = [0, 64] \times [0, 64] \times [0, 64]$, $\tau = 1.0 \times 10^{-2}$.

do not have an exact solution, instead of calculating the error at the final time, we compute the Cauchy difference, which is defined as $\delta_\phi := \phi_{h_f} - \mathcal{I}_c^f(\phi_{h_c})$, where $\mathcal{I}_c^f$ is a bilinear interpolation operator (We applied Nearest Neighbor Interpolation in Matlab, which is similar to the 2D case in [47,48]). This requires having a relatively coarse solution, parametrized by h_c, and a relatively fine solution, parametrized by h_f, where $h_c = 2h_f$, at the same final time. The ℓ^2 norms of Cauchy difference and the convergence rates can be found in Table 1. The results confirm our expectation for the convergence order. Moreover, the

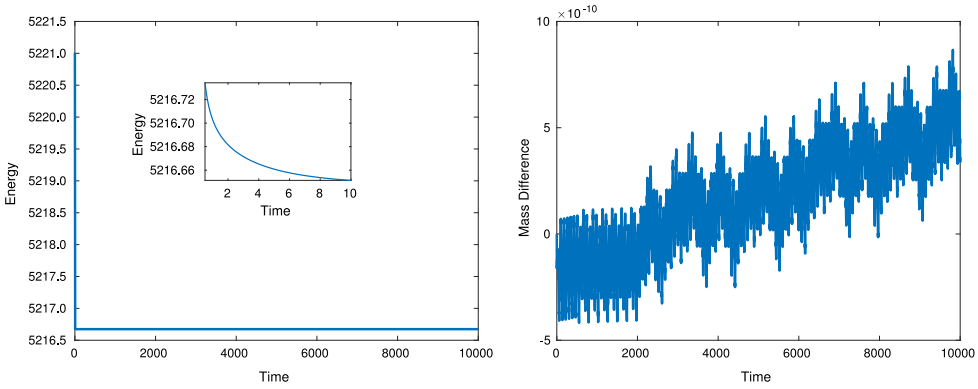

Fig. 4. The plots of energy evolution and mass difference depicted in Fig. 3.

plots of the energy and mass difference evolution indicate that the energy is non-increasing and the mass is conservative, up to a tolerance of 10^{-10}, for the simulation with initial condition (6.1) (see Fig. 1).

Remark 6.1. When calculating the Cauchy difference between the two different grids, the interpolation operator should be consistent with the discrete stencil, otherwise the optimal convergence rate may not be observed. We applied Nearest Neighbor Interpolation in Matlab.

In the second part of this test, we investigate the complexity of the multigrid solver. The number of multigrid iterations to reach the residual tolerance is given in Table 2, for various choices of grid sizes and (ν_1, ν_2). Table 2 indicates that the iteration numbers are nearly independent on h, when we use 2 pre-smoothing and 2 post-smoothing. The detailed reduction in the norm of the residual for each V-cycle iteration at the 10th time step can be found in Fig. 2. As can be seen, the norm of the residual of each V-cycle is reduced by approximately the same rate each time with $\nu_1 = \nu_2 = 2$, regardless of h. This is a typical feature of multigrid when it is operating with optimal complexity [42,45,49]. For $\nu_1 = \nu_2 = 1$, we do not observe a similar feature. Moreover, we also observe that more multigrid iterations are required for smaller values of h, which confirms our convergence analysis.

6.2. Growth of a polycrystal

The initial data for this simulation are taken as essentially random:

$$\phi^0_{i,j,k} = 0.2 + 0.005 \cdot r_{i,j,k}, \tag{6.2}$$

where the $r_{i,j,k}$ are uniformly distributed random numbers in [0, 1]. We use $\varepsilon = 2.5 \times 10^{-1}$, and $L = 64$ (in the simulation shown in Fig. 3) and $L = 128$ (in the simulation shown in Fig. 5). Time snapshots of the micro-structure can be found in Figs. 3 and 5, which display the transition between the liquid and solid states with random initial liquid density. The numerical results are consistent with the experiments on this topic in [37]. The corresponding energy and mass difference evolution depicted in Fig. 3 are presented in Fig. 4.

7. Conclusions

In this paper, we have provided a detailed convergence analysis of a finite difference scheme for the three-dimensional PFC equation, with the second order accuracy in both time and space established. The numerical scheme was proposed in [21], with the unique solvability and unconditional energy stability already proved in the earlier work. Meanwhile, a theoretical justification of the convergence analysis turns out to be challenging, due to a difficulty to obtain a maximum norm bound of the numerical solution in three-dimensional space. We overcome this difficulty with the help of discrete Fourier transformation, and repeated applications of Parseval equality in both continuous and discrete spaces. With such a discrete maximum norm bound developed for the numerical solution, the convergence analysis could be derived by a careful process of consistency estimate and stability analysis for the numerical error function.

In addition, we describe the detailed multigrid solver to implement this numerical scheme over a three-dimensional domain. Various numerical results are presented, including the numerical convergence test and the three-dimensional polycrystal growth simulation. The efficiency and robustness of the nonlinear multigrid solver has been extensively demonstrated in these three-dimensional numerical experiments.

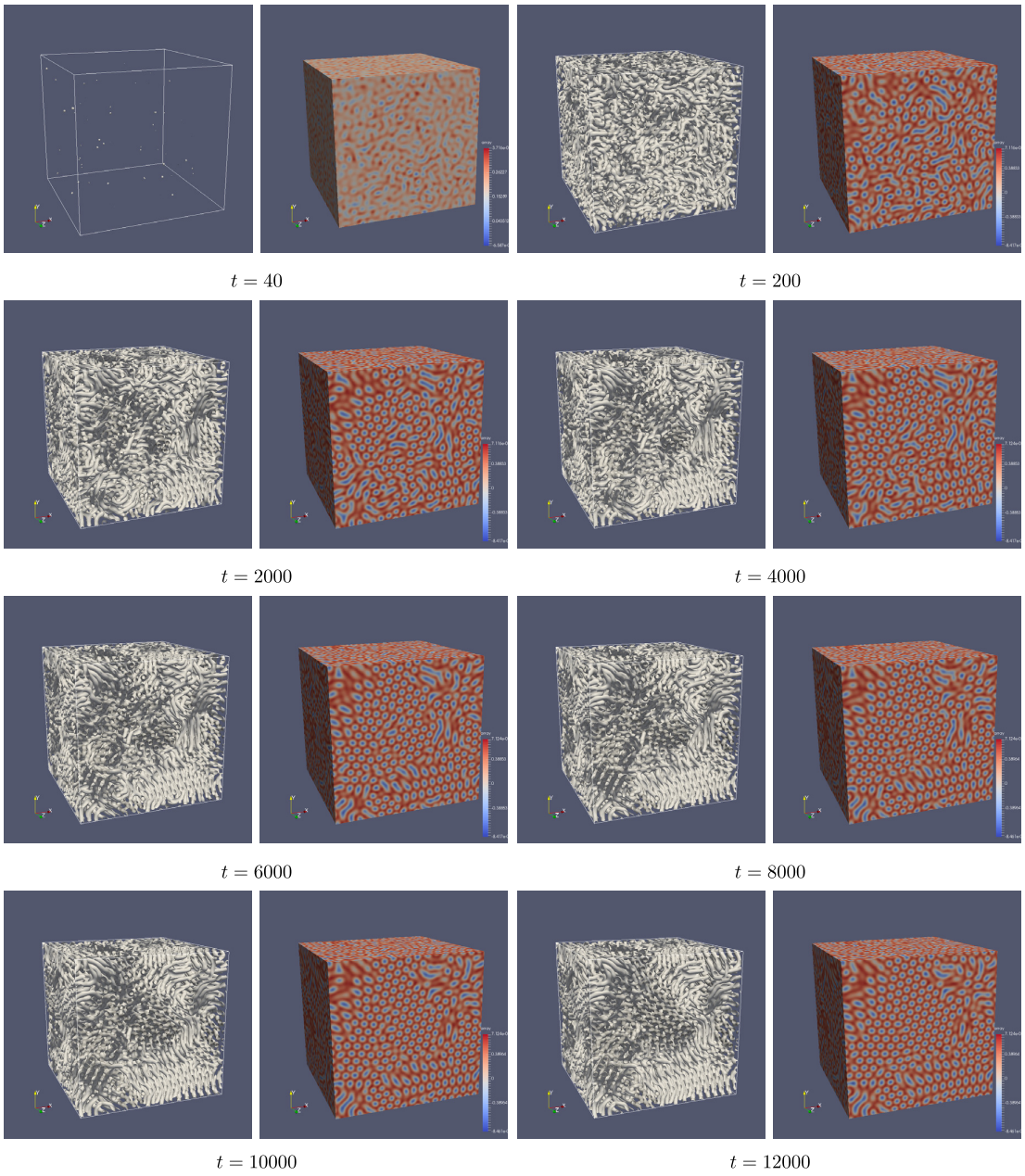

Fig. 5. Three-dimensional periodic micro-structures snapshots with initial condition (6.2) at $t = 40, 200, 2000, 4000, 6000, 8000, 10\,000$ and $12\,000$. Left: iso-surface plots of $\phi = 0.0$, Right: snapshots of micro-structures plots. The parameters are $\varepsilon = 2.5 \times 10^{-1}$, $h = 128/128 = 1.0$, $\Omega = [0, 128] \times [0, 128] \times [0, 128]$, $\tau = 1.0 \times 10^{-2}$.

Acknowledgments

The second author would like to thank Jing Guo at South China University of Technology for the valuable discussions. This work is supported in part by NSF DMS-1418689 (C. Wang), NSF DMS-1418692 (S. Wise), NSFC 11271048, 11571045 and the Fundamental Research Funds for the Central Universities (Z. Zhang).

Appendix. The discrete Gronwall inequality

We need the following discrete Gronwall inequality cited in [44]:

Lemma A.1. *Fix $T > 0$. Let M be a positive integer, and define $\tau \leq \frac{T}{M}$. Suppose $\{a_m\}_{m=0}^{M}$, $\{b_m\}_{m=0}^{M}$ and $\{c_m\}_{m=0}^{M-1}$ are non-negative sequences such that $\tau \sum_{m=0}^{M-1} c_m \leq C_1$, where C_1 is independent of τ and M. Further suppose that,*

$$a_\ell + \tau \sum_{m=0}^{\ell} b_m \leq C_2 + \tau \sum_{m=0}^{\ell-1} a_m c_m, \quad \forall\, 1 \leq \ell \leq M, \tag{A.1}$$

where $C_2 > 0$ is a constant independent of τ and M. Then, for all $\tau > 0$,

$$a_\ell + \tau \sum_{m=0}^{\ell} b_m \leq C_2 \exp\left(\tau \sum_{m=0}^{\ell-1} c_m\right) \leq C_2 \exp(C_1), \quad \forall\, 1 \leq \ell \leq M. \tag{A.2}$$

References

[1] K. Elder, M. Katakowski, M. Haataja, M. Grant, Modeling elasticity in crystal growth, Phys. Rev. Lett. 88 (2002) 245701.
[2] K. Elder, M. Grant, Modeling elastic and plastic deformations in nonequilibrium processing using phase filed crystal, Phys. Rev. E 90 (2004) 051605.
[3] P. Stefanovic, M. Haataja, N. Provatas, Phase-field crystals with elastic interactions, Phys. Rev. Lett. 96 (2006) 225504.
[4] K. Elder, N. Provatas, J. Berry, P. Stefanovic, M. Grant, Phase-field crystal modeling and classical density functional theory of freezing, Phys. Rev. B 77 (2007) 064107.
[5] N. Provatas, J. Dantzig, B. Athreya, P. Chan, P. Stefanovic, N. Goldenfeld, K. Elder, Using the phase-field crystal method in the multiscale modeling of microstructure evolution, JOM 59 (2007) 83.
[6] R. Backofen, A. Rätz, A. Voigt, Nucleation and growth by a phase field crystal (PFC) model, Phil. Mag. Lett. 87 (2007) 813.
[7] U. Marconi, P. Tarazona, Dynamic density functional theory of liquids, J. Chem. Phys. 110 (1999) 8032.
[8] K. Elder, N. Provatas, Amplitude expansion of the binary phase-field-crystal model, Phys. Rev. E 81 (1) (2010) 011602.
[9] P. Stefanovic, M. Haataja, N. Provatas, Phase field crystal study of deformation and plasticity in nanocrystalline materials, Phys. Rev. E 80 (2009) 046107.
[10] Z. Guan, V. Heinonen, J. Lowengrub, C. Wang, S. Wise, An energy stable, hexagonal finite difference scheme for the 2D phase field crystal amplitude equations, J. Comput. Phys. 321 (2016) 1026–1054.
[11] J. Swift, P. Hohenberg, Hydrodynamic fluctuations at the convective instability, Phys. Rev. A 15 (1977) 319.
[12] C. Wang, S. Wise, Global smooth solutions of the modified phase field crystal equation, Methods Appl. Anal. 17 (2010) 191–212.
[13] M. Cheng, J. Warren, An efficient algorithm for solving the phase field crystal model, J. Comput. Phys. 227 (2008) 6241.
[14] B. Vollmayr-Lee, A. Rutenberg, Fast and accurate coarsening simulation with an unconditionally stable time step, Phys. Rev. E 68 (2003) 066703.
[15] G. Tegze, G. Bansel, G. Tóth, T. Pusztai, Z. Fan, L. Gránásy, Advanced operator splitting-based semi-implicit spectral method to solve the binary phase-field crystal equations with variable coefficients, J. Comput. Phys. 228 (2009) 1612–1623.
[16] B. Athreya, N. Goldenfeld, J. Dantzig, M. Greenwood, N. Provatas, Adaptive mesh computation of polycrystalline pattern formation using a renormalization-group reduction of the phase-field crystal model, Phys. Rev. E 76 (2007) 056706.
[17] H. Cao, Z. Sun, Two finite difference schemes for the phase field crystal equation, Sci. China Math. 58 (11) (2015) 2435–2454.
[18] R. Guo, Y. Xu, Local discontinuous galerkin method and high order semi-implicit scheme for the phase field crystal equation, SIAM J. Sci. Comput. 38 (1) (2016) A105–A127.
[19] T. Hirouchi, T. Takaki, Y. Tomita, Development of numerical scheme for phase field crystal deformation simulation, Comput. Mater. Sci. 44 (2009) 1192–1197.
[20] D. Eyre, Unconditionally gradient stable time marching the Cahn-Hilliard equation, in: J.W. Bullard, R. Kalia, M. Stoneham, L. Chen (Eds.), Computational and Mathematical Models of Microstructural Evolution, Vol. 53, Materials Research Society, Warrendale, PA, USA, 1998, pp. 1686–1712.
[21] Z. Hu, S. Wise, C. Wang, J. Lowengrub, Stable and efficient finite-difference nonlinear-multigrid schemes for the phase-field crystal equation, J. Comput. Phys. 228 (2009) 5323–5339.
[22] A. Baskaran, Z. Hu, J. Lowengrub, C. Wang, S. Wise, P. Zhou, Energy stable and efficient finite-difference nonlinear multigrid schemes for the modified phase field crystal equation, J. Comput. Phys. 250 (2013) 270–292.
[23] A. Baskaran, J. Lowengrub, C. Wang, S. Wise, Convergence analysis of a second order convex splitting scheme for the modified phase field crystal equation, SIAM J. Numer. Anal. 51 (2013) 2851–2873.
[24] J. Bueno, I. Starodumov, H. Gomez, P. Galenko, D. Alexandrov, Three dimensional structures predicted by the modified phase field crystal equation, Comput. Mater. Sci. 111 (2016) 310–312.
[25] M. Grasselli, M. Pierre, Energy stable and convergent finite element schemes for the modified phase field crystal equation, ESAIM: M2AN 50 (5) (2016) 1523–1560.
[26] C. Wang, S. Wise, An energy stable and convergent finite-difference scheme for the modified phase field crystal equation, SIAM J. Numer. Anal. 49 (2011) 945–969.
[27] S. Wise, C. Wang, J. Lowengrub, An energy stable and convergent finite-difference scheme for the phase field crystal equation, SIAM J. Numer. Anal. 47 (2009) 2269–2288.
[28] A. Christlieb, J. Jones, K. Promislow, B. Wetton, M. Willoughby, High accuracy solutions to energy gradient flows from material science models, J. Comput. Phys. 257 (2014) 193–215.
[29] F. Guillén-González, G. Tierra, Second order schemes and time-step adaptivity for Allen-Cahn and Cahn-Hilliard models, Comput. Math. Appl. 68 (8) (2014) 821–846.
[30] X. Yang, D. Han, Linearly first- and second-order, unconditionally energy stable schemes for the phase field crystal equation, J. Comput. Phys. 330 (2017) 1116–1134.
[31] D. Han, A. Brylev, X. Yang, Z. Tan, Numerical analysis of second order, fully discrete energy stable schemes for phase field models of two phase incompressible flows, J. Sci. Comput. (2016) 1–25.
[32] X. Yang, Linear, and unconditionally energy stable numerical schemes for the phase field model of homopolymer blends, J. Comput. Phys. 302 (2016) 509–523.

[33] J. Zhao, Q. Wang, X. Yang, Numerical approximations for a phase field dendritic crystal growth model based on the invariant energy quadratization approach, Internat. J. Numer. Methods Engrg. 110 (3) (2017) 279–300.
[34] A. Diegel, C. Wang, S. Wise, Stability and convergence of a second order mixed finite element method for the Cahn-Hilliard equation, IMA J. Numer. Anal. 36 (2016) 1867–1897.
[35] J. Guo, C. Wang, S. Wise, X. Yue, An H^2 convergence of a second-order convex-splitting, finite difference scheme for the three-dimensional Cahn-Hilliard equation, Commun. Math. Sci. 14 (2016) 489–515.
[36] M. Dehghan, V. Mohammadi, The numerical simulation of the phase field crystal (PFC) and modified phase field crystal (MPFC) models via global and local meshless methods, Comput. Methods Appl. Mech. Engrg. 298 (2016) 453–484.
[37] H. Gomez, X. Nogueira, An unconditionally energy-stable method for the phase field crystal equation, Comput. Methods Appl. Mech. Engrg. 249 (2012) 52–61.
[38] Z. Zhang, Y. Ma, Z. Qiao, An adaptive time-stepping strategy for solving the phase field crystal model, J. Comput. Phys. 249 (2013) 204–215.
[39] C. Collins, J. Shen, S. Wise, An efficient, energy stable scheme for the Cahn-Hilliard-Brinkman system, Commun. Comput. Phys. 13 (2013) 929–957.
[40] Z. Guan, J. Lowengrub, C. Wang, S. Wise, Second-order convex splitting schemes for nonlocal Cahn-Hilliard and Allen-Cahn equations, J. Comput. Phys. 277 (2014) 48–71.
[41] Z. Guan, C. Wang, S. Wise, A convergent convex splitting scheme for the periodic nonlocal Cahn-Hilliard equation, Numer. Math. 128 (2014) 377–406.
[42] S. Wise, Unconditionally stable finite difference, nonlinear multigrid simulation of the Cahn-Hilliard-Hele-Shaw system of equations, J. Sci. Comput. 44 (2010) 38–68.
[43] L. Trefethen, Spectral Methods in MATLAB, Vol. 10, SIAM, 2000.
[44] J.G. Heywood, R. Rannacher, Finite element approximation of the nonstationary Navier-Stokes problem. IV. Error analysis for the second-order time discretization, SIAM J. Numer. Anal. 27 (1990) 353–384.
[45] U. Trottenberg, C.W. Oosterlee, A. Schuller, Multigrid, Academic Press, 2000.
[46] W. Feng, Z. Guo, J. Lowengrub, S. Wise, Mass-conservative cell-centered finite difference methods and an efficient multigrid solver for the diffusion equation on block-structured, locally cartesian adaptive grids, 2016 (in preparation).
[47] W. Feng, Z. Guan, J. Lowengrub, S. Wise, C. Wang, An energy stable finite-difference scheme for functionalized Cahn–Hilliard Equation and its convergence analysis, 2016, arXiv preprint arXiv:1610.02473.
[48] W. Feng, A. Salgado, C. Wang, S. Wise, Preconditioned steepest descent methods for some nonlinear elliptic equations involving p-Laplacian terms, J. Comput. Phys. 334 (2017) 45–67.
[49] D. Kay, R. Welford, A multigrid finite element solver for the Cahn-Hilliard equation, J. Comput. Phys. 212 (1) (2006) 288–304.